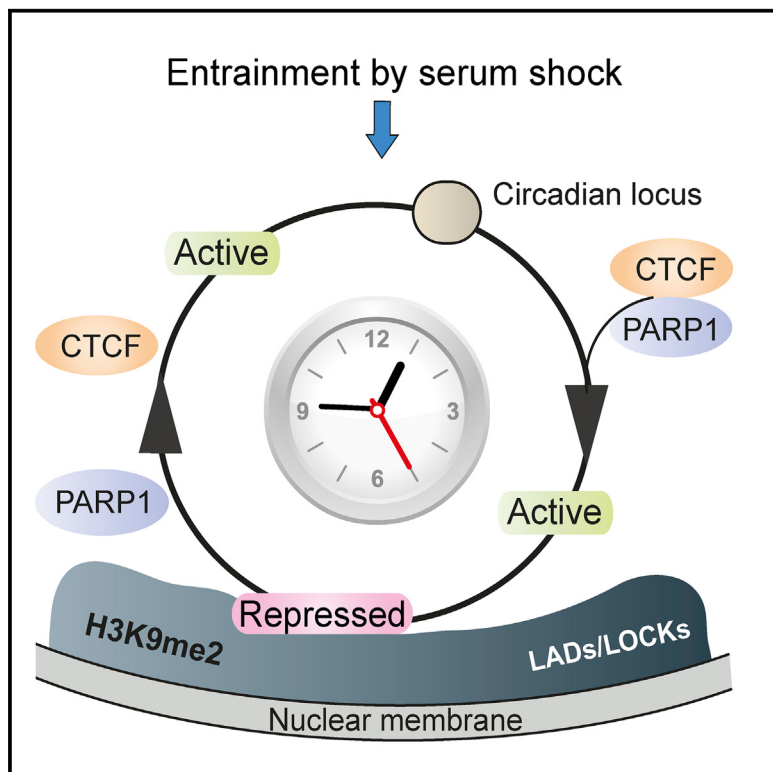


# Molecular Cell

## PARP1- and CTCF-Mediated Interactions between Active and Repressed Chromatin at the Lamina Promote Oscillating Transcription

### Graphical Abstract



### Authors

Honglei Zhao, Emmanouil G. Sifakis,  
Noriyuki Sumida, ..., Thomas Helleday,  
Márta P. Imreh, Anita Göndör

### Correspondence

anita.gondor@ki.se

### In Brief

Zhao et al. show that entrainment of the circadian rhythm by serum shock induces the circadian recruitment of clock-controlled genes to the repressive environment of the nuclear periphery, leading to diurnal transcriptional attenuation. PARP1 and CTCF regulate the contacts between clock-controlled genes and lamina-associated chromatin as well as oscillating transcription.

### Highlights

- CTCF and PARP1 regulate contacts between clock-controlled genes and LADs
- Serum shock induces diurnal CTCF-PARP1 binding and circadian gene-lamina contacts
- The repressive milieu of the lamina promotes circadian transcriptional attenuation
- Depletion of PARP1, CTCF, or H3K9me2/3 antagonizes oscillating transcription

### Accession Numbers

GSE26880  
GSE58534

# PARP1- and CTCF-Mediated Interactions between Active and Repressed Chromatin at the Lamina Promote Oscillating Transcription

Honglei Zhao,<sup>1,5</sup> Emmanouil G. Sifakis,<sup>1,5</sup> Noriyuki Sumida,<sup>1,5</sup> Lluís Millán-Ariño,<sup>1,5</sup> Barbara A. Scholz,<sup>1</sup> J. Peter Svensson,<sup>2</sup> Xingqi Chen,<sup>1</sup> Anna L. Ronnegren,<sup>1</sup> Carolina Dietrich Mallet de Lima,<sup>1</sup> Farzaneh Shahin Varnoosfaderani,<sup>1</sup> Chengxi Shi,<sup>1,6</sup> Olga Loseva,<sup>3</sup> Samer Yammine,<sup>1</sup> Maria Israelsson,<sup>1</sup> Li-Sophie Rathje,<sup>1</sup> Balázs Németi,<sup>1,4</sup> Erik Fredlund,<sup>1,7</sup> Thomas Helleday,<sup>3</sup> Márta P. Imreh,<sup>1</sup> and Anita Göndör,<sup>1,\*</sup>

<sup>1</sup>Department of Microbiology, Tumor and Cell Biology, Nobels väg 16, Karolinska Institutet, 17177 Stockholm, Sweden

<sup>2</sup>Department of Biosciences and Nutrition, Novum, Karolinska Institutet, 14183 Huddinge, Sweden

<sup>3</sup>Science for Life Laboratory, Division of Translational Medicine and Chemical Biology, Department of Medical Biochemistry and Biophysics, Karolinska Institutet, 17121 Stockholm, Sweden

<sup>4</sup>Department of Pharmacology and Pharmacotherapy, Faculty of Medicine, University of Pécs, Szigeti út 12, 7624 Pécs, Hungary

<sup>5</sup>Co-first author

<sup>6</sup>Present address: China Overseas Plaza, 8 Guanghuadongli, Jianguomenwai Avenue, Chaoyang District, Beijing 100020, China

<sup>7</sup>Present address: Department of Oncology and Pathology, Karolinska Institutet, 171 76 Stockholm, Sweden

\*Correspondence: anita.gondor@ki.se

<http://dx.doi.org/10.1016/j.molcel.2015.07.019>

## SUMMARY

Transcriptionally active and inactive chromatin domains tend to segregate into separate sub-nuclear compartments to maintain stable expression patterns. However, here we uncovered an inter-chromosomal network connecting active loci enriched in circadian genes to repressed lamina-associated domains (LADs). The interactome is regulated by PARP1 and its co-factor CTCF. They not only mediate chromatin fiber interactions but also promote the recruitment of circadian genes to the lamina. Synchronization of the circadian rhythm by serum shock induces oscillations in PARP1-CTCF interactions, which is accompanied by oscillating recruitment of circadian loci to the lamina, followed by the acquisition of repressive H3K9me2 marks and transcriptional attenuation. Furthermore, depletion of H3K9me2/3, inhibition of PARP activity by olaparib, or downregulation of PARP1 or CTCF expression counteracts both recruitment to the envelope and circadian transcription. PARP1- and CTCF-regulated contacts between circadian loci and the repressive chromatin environment at the lamina therefore mediate circadian transcriptional plasticity.

## INTRODUCTION

Genomic functions influence and are influenced by the arrangement of the genome within the 3D space of the nucleus (Göndör and Ohlsson, 2009; Bickmore and van Steensel, 2013). An important hallmark of the nuclear architecture is the dynamic

spatial separation of active and inactive chromatin domains (Bickmore and van Steensel, 2013; Nagano et al., 2013), which is exemplified by the juxtaposition of active transcriptional units in transcription factories (Xu and Cook, 2008; Schoenfelder et al., 2010) and the cell type-specific coordination of repressed states at the lamina (Reddy and Feinberg, 2013).

The formation of the transcriptionally repressive environment at the nuclear envelope is linked to the acquisition of large blocks of repressive histone modifications, such as histone 3 lysine 9 di- and trimethylation (H3K9me2 and H3K9me3, respectively) (Towbin et al., 2012; Wen et al., 2009) at the so-called lamina-associated domains (LADs) (Reddy and Feinberg, 2013; Bickmore and van Steensel, 2013; Nagano et al., 2013) that contain the AT-rich, repressed portion of the genome and developmentally silenced genes. Dynamic interactions between chromatin and the lamina are controlled by repressive histone modifications (Guelen et al., 2008; Towbin et al., 2012) and sequence-specific transcription factors (Zullo et al., 2012). The emerging separation of active and repressed environments is considered to promote robust cell type-specific expression repertoires by preventing the erosion of epigenetic states (Reddy and Feinberg, 2013) and spatially constraining stochastic encounters between regulatory elements (Göndör and Ohlsson, 2009; Reddy and Feinberg, 2013).

Dynamic transcriptional changes likely require flexible higher-order structures to enable a prompt response to changing microenvironments. The underlying protein-protein and protein-nucleic acid interactions mediating the transcriptional response are therefore typically regulated by differential distribution of factors within the cell/nucleus and reversible post-translational modifications, such as the addition of multiple ADP-ribose (PAR) units by PAR polymerases (PARPs) to nuclear proteins (Krishnakumar and Kraus, 2010; Tallis et al., 2014; Beneke, 2012). Importantly, PARylation of the transcription factor CTCF, a major regulator of transcriptional

coordination in three dimensions (Ong and Corces, 2014; Ohlsson et al., 2010), is required for its function as an insulator (Yu et al., 2004).

A paradigm of adaptive transcriptional plasticity is represented by the circadian control of gene expression. Cell-autonomous clocks regulated by auto-regulatory feedback loops, time delays, and post-translational modifications generate daily oscillations in the transcriptome and proteome (Asher and Schibler, 2011; Sahar and Sassone-Corsi, 2012; Takahashi et al., 2008). Periodic oscillations of gene products controlling cell signaling and metabolism contribute to timing-dependent combinatorial patterns in the proteome of single cells that may synergize or antagonize the effects of environmental cues on the cell (Janich et al., 2011).

The core clock system of peripheral cells is composed of transcriptional activators (BMAL1 and CLOCK) that activate clock-controlled genes, among them genes coding for factors (CRY/PER and REV-ERBs) that inhibit the activators via negative feedback loops (Zhang and Kay, 2010; Cho et al., 2012). External time cues synchronize the cell-autonomous clocks with the geophysical time within an organism or a cell population. The two main external time cues are light/dark and feeding/fasting cycles. Feeding exerts a dominant effect on the entrainment of peripheral clocks (Balsalobre et al., 1998), where PARP1 plays essential roles (Asher et al., 2010).

Circadian regulation is likely to be influenced by the 3D context of the responsive genes (Aguilar-Arnal et al., 2013). To gain insight into the principles regulating the dynamics and function of 3D chromatin crosstalk, the circular chromosome conformation capture (4C) technique (Zhao et al., 2006; Göndör et al., 2008) was employed to map the topology of the chromatin fiber network impinging on a CTCF- and PARP1-occupied regulatory region, the *H19* imprinting control region (ICR), which resides in a domain under circadian control (Shi et al., 2013). Strikingly, this interactome differed from other published chromatin networks (Bickmore and van Steensel, 2013) because it was dominated by inter-chromosomal interactions that connected active loci, enriched in circadian genes, with repressed LADs. PARP1, together with its cofactor CTCF, emerged as major organizers of the interactome by regulating chromatin interactions as well as chromatin mobility between different sub-nuclear compartments. Recruitment of circadian chromatin hubs to the nuclear envelope displayed 24-hr oscillations upon serum shock, linked with circadian attenuation of transcription. We suggest that PARP1 and CTCF are regulators of interactions between active and inactive nuclear compartments to connect oscillating 3D chromatin conformations with the metabolic states of the cell (Becker et al., 2004).

## RESULTS

### An Inter-chromosomal Interactome Connects Active Transcription Units to Repressed Domains

Using the *H19* ICR as bait, 4C sequencing analysis of human embryonic stem cells (hESCs) and derived embryoid bodies (hEBs) identified 518 different regions (Table S1) that reproduc-

ibly interacted with the *H19* ICR (Figure 1A; Figures S1A and S1B) in a developmentally regulated manner (Figure S1C). Interestingly, the *H19* ICR interactome was dominated by inter-chromosomal interactions (Figure 1B), which was further validated by 3D DNA fluorescence in situ hybridization (FISH) analyses measuring physical distances between the bait and its interactors. Therefore, interactors having high read counts in the 4C sequencing (4C-seq) analyses were significantly closer to the bait than sequences with low read counts, indicating increased or decreased potentials for interaction, respectively (Figure 1C). The sequences within the 4C libraries contained both genes and inter-genic regions (Figure 1D) with an enrichment for transcriptional units (Figure 1E) controlling cell adhesion/synaptic processes (Table S2).

To examine the topology of the network, we took advantage of the unique capacity of our 4C assay to capture more than two simultaneously interacting sequences during the formation of the circular ligation products (Zhao et al., 2006; Göndör et al., 2008). The “bridges” connecting simultaneously interacting sequences (Figure 1F; Table S1) were used to re-construct the interactions between the interactors of the *H19* ICR. The sum of all interactions within the interactome (Figure 1G) formed a network with high modularity (Figure 1H) and an approximate scale-free topology (Figure S1D). Although interactions within the network were dynamic, with considerable cellular heterogeneity in interaction frequencies, nodes with multiple interactions emerged reproducibly in multiple 4C samples (Figure S1E). The network topology was further validated by 4C analysis using VAT1L (encoding a vesicle amine transport 1-like protein with oxidoreductase activity)—the chromatin hub connected to every module of the *H19* ICR interactome (arrow, Figure 1H)—as new bait. The results confirmed the VAT1L-*H19* ICR interaction (Table S1) and identified many other genomic loci that interacted independently with *H19* ICR (Figure 1I). The *H19* ICR network also displayed features of being regulated, such as higher-than-expected transitivity, average shortest path length, and assortativity coefficient by degree (Figure S1F). Finally, 3D DNA FISH confirmed that physical proximity between interacting nodes (Table S3) was more frequent than the proximity between regions further apart in the network (Figures 1J and 1K). The frequent proximities between network nodes without the simultaneous presence of the *H19* ICR indicated that the *H19* ICR was in contact with only a selected set of regions at any given time, which themselves frequently interacted with other loci. Examples of DNA FISH images of pairwise and multiple proximities are displayed in Figures S1G–S1L.

A striking feature of the inter-chromosomal network was that various chromatin states, ranging from inactive (repressed, heterochromatin) to active (enhancers, transcriptional elongation), mixed within each of the modules (Figures 1L and 1M; Table S4), ruling out a function in transcriptional coordination in transcription factories. Nearest neighbor analysis showed that active and inactive regions did not segregate away from each other within the network (Figure 1N). Furthermore, the assortativity coefficient by transcriptional activity, a measure of the level of segregation between active and inactive nodes, indicated no preference for interactions between active loci in the interactome (Figure 1O).

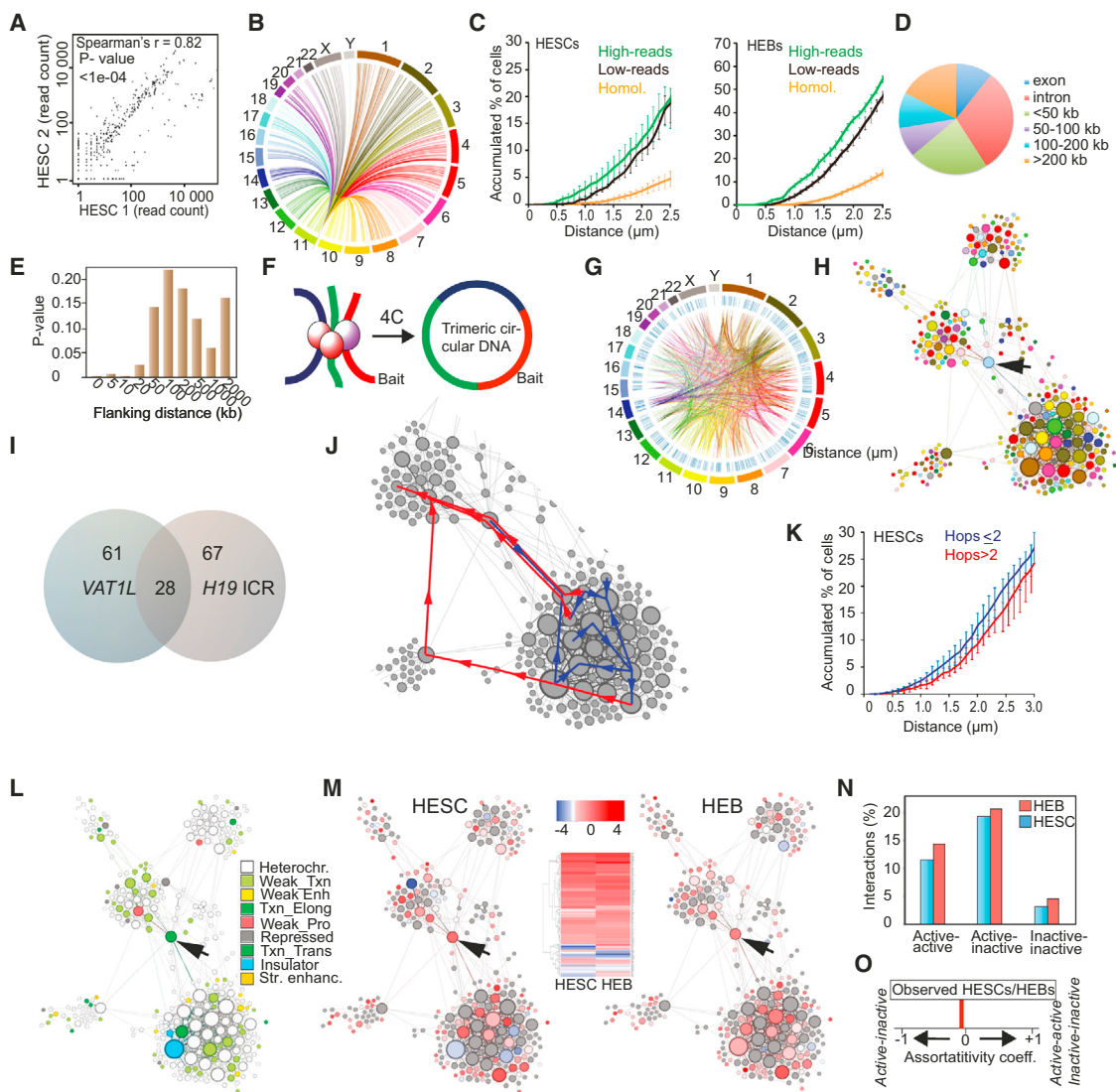


**Figure 1. The Topology of the Chromosome Interactome Impinging on the H19 ICR**

(A) Reproducibility of the 4C-seq (Solexa) analysis. The scatterplot compares read counts of H19 ICR interactors emerging in biological duplicates of hESCs samples.

(B) Circos plot illustrating the inter-chromosomal character of the H19 ICR interactome in hESCs and hEBs.

(C) DNA FISH analysis comparing the accumulated physical distances between the H19 ICR and its interactors having high (green) versus low (black) read counts in the 4C-seq as well as between homologous alleles (orange) (Table S3). 200 alleles were counted in duplicate experiments. Data are represented as mean  $\pm$  SEM. Two-sample, two-tailed Mann-Whitney U tests between the proximity of the H19/IGF2 locus and high or low read count interactors showed a statistically significant difference with  $p \leq 0.05$  for both hESCs and hEBs (Figure S1L).

(D) Pie chart demonstrating the distribution of H19 ICR interactors in the genome.

(E) Transcriptional units are over-represented among the interactors of H19 ICR up to a 20-kb flanking distance.

(F) The principle of the 4C assay enabling the identification of multiple interactions.

(G) Circos plot representation of the topology of the H19 ICR network.

(H) Visualization of the network topology by Gephi. See (G) for the color code. The arrow indicates VAT1L connecting all modules.

(I) Overlap between the interactors of the H19 ICR and the VAT1L baits as identified by MiSeq desktop sequencer analysis of hESC 4C samples.

(J and K) Schematic (J) of the interactors chosen in (K) showing physical distances between proximal nodes (i.e., hops  $\leq 2$ ) and distant nodes (hops  $> 2$ ) analyzed by 3D DNA FISH. The arrows indicate the number of connecting nodes between the examined chromatin hubs. Two-sample, two-tailed Mann-Whitney U tests showed a statistically significant difference in DNA FISH proximity between proximal interactors (hops  $\leq 2$ ) and distal interactors (hops  $> 2$ ). The lowest calculated p value was identified at distances within 1.2  $\mu\text{m}$  ( $p \leq 0.01$ ). 200 alleles were counted in duplicate experiments. Data are represented as mean  $\pm$  SEM. See also Figures S1K and S1L.

(L) The distribution of chromatin states within the network shown in (H) was assessed based on the chromatin state segmentation by hidden Markov model (HMM) from the Encyclopedia of DNA Elements (ENCODE)/Broad and using the original color code as in Ernst et al. (2011). Txn, transcription/transcription; Heterochr, heterochromatin; Enh, enhancer; Elong, elongation; Pro, promoter; Trans, transition; Str Enhanc, strong enhancer.

(legend continued on next page)

## CTCF and PARP1 Interactions Regulate the *H19* ICR Chromatin Fiber Interactome

As the reproducibility of the *H19* ICR interactome suggested regulated encounters between network nodes, we decided to identify the dynamic molecular ties of the network. Because PARylation of CTCF at the maternal *H19* ICR allele is essential for long-range chromatin insulation in *cis* (Yu et al., 2004), we hypothesized that PARP activity might also contribute to the organization of chromatin networks in *trans*. To test whether PAR was present at the time of interaction, PAR was depleted from formaldehyde cross-linked chromatin by PAR glycohydrolase (PARG), followed by 4C-seq (Figure 2A). Because our 4C technique is highly reproducible (Figure 1A; Figures S1A and S1B), the effect of PARG could be reliably assessed. Strikingly, the removal of PAR led to the disassembly of the majority of interactors from the *H19* ICR in both hESCs and hEBs (Figure 2B; Figures S2A–S2D). Potential contamination of feeder cells was less than 1% and 0.1%, respectively (Supplemental Experimental Procedures; Figures S2E–S2H), indicating that the presence of PAR in the chromatin preparations was specific to hESCs and hEBs. Finally, because RNase treatment of crosslinked chromatin did not reproduce the effects of PARG (Figure S2I), we concluded that the PARG effect (Figures S2A–S2D) did not depend on any RNase contamination.

To examine the mechanism of PAR deposition on chromatin, we revisited the observation that CTCF is able to activate PARP1 (Guastafierro et al., 2008). As illustrated in Figures S2J–S2M, CTCF activated PARP1, but not PARP3, in a concentration-dependent manner in the absence of activating DNA. This indicates that PARylation in chromatin complexes might be due to functional CTCF-PARP1 interactions. Indeed, downregulation of CTCF expression correlated with reduced cellular PAR levels (Figures S2N and S2O), suggesting that CTCF is a major regulator of PARP1. Furthermore, chromatin immunoprecipitation (ChIP) analysis illustrated that PARP1 bound to the same parental *H19* ICR allele as CTCF (Figures 2C and 2D; Table S5), supporting its involvement in the assembly of the interactome.

To probe the possibility that the inter-chromosomal network was established by initial CTCF-PARP1 interactions, we examined the presence of PARP1 at the time of interaction between the *H19* ICR and *VAT1L*. ChIP-loop assay (Figure 2E) illustrated that a PARP1 antibody pulled down interacting *H19* ICR-VAT1L complexes. Furthermore, 3D DNA FISH revealed that treating hESCs with olaparib (primarily an inhibitor for PARP1; Pettitt et al., 2013) for 24 hr significantly reduced the proximity between *IGF2/H19* and *VAT1L* as well as between *IGF2/H19* and a circadian chromatin hub, *PARD3* (PAR3 family cell polarity regulator) (Figure 2F). In line with this observation, ola-

parib affected the relative positions of *VAT1L* and *IGF2/H19* with respect to their chromosome territories (Figures S2P and S2Q), suggesting that PARP activity also affects chromatin movements.

In parallel, ChIP analyses revealed that PARP1 and PAR were enriched at the *VAT1L* node in hESCs even though they were also present at the *H19* ICR and other chromatin hubs (Figure 2G; Figure S2R; Table S5). CTCF occupancy, on the other hand, was prominent at the *H19* ICR with levels of CTCF binding varying at other chromatin hubs (Figure 2G; Table S5). Strikingly, 24-hr treatment of hESCs with olaparib reduced the weak CTCF signal at the *VAT1L* locus and other chromatin hubs while leaving CTCF binding to the *H19* ICR unaffected (Figure 2G; Figure S2R; Table S5). Conversely, olaparib evicted PARP1 almost completely from all nodes examined, including the bait (Figure 2G; Table S5). The implications of these results are two-fold. First, they raise the possibility that the weak CTCF binding at the interactors of the *H19* ICR represent indirect CTCF binding mediated via interactions with CTCF-occupied loci. Second, they suggest that olaparib directly affects CTCF-PARP1 binding and, thereby, disrupts chromatin fiber interactions.

To examine this issue, CTCF was immunoprecipitated either from an *in vitro* mixture of recombinant CTCF and PARP1 or from nuclear lysates with or without olaparib, followed by western blot analysis of a PARP1 epitope. Incubation of recombinant CTCF-PARP1 complexes with olaparib for 10 min or including olaparib during coimmunoprecipitation (co-IP) from cell lysates was sufficient to disrupt the interactions between CTCF and PARP1 (Figures 3A and 3B). Additionally, ChIP analysis demonstrated that incubation of hESC chromatin with olaparib during the fixation step for 10 min decreased PARP1 binding both to the *H19* ICR and *VAT1L* (Figure 3C). Moreover, even though an *in situ* proximity ligation assay (ISPLA) visualized extensive CTCF-PARP1 proximities in control hESCs, olaparib presence during crosslinking disrupted CTCF-PARP1 proximities (Figure 3D). Finally, in line with the assumption that the network between the *H19* ICR and its interactors was built on initial CTCF-PARP1 interactions, 4C analysis illustrated that a 10-min incubation with olaparib during the crosslinking step disassembled most of the interactions between the bait and its interactors in hESCs (Figure 3E), resembling the effects of 24-hr olaparib treatment (Figures S3A and S3B).

Based on these results, we propose a model where chromatin hubs of the inter-chromosomal network located within shared chromosomal domains (Figure 3F) are likely connected to the *H19* ICR via CTCF-PARP1 interactions (Figure 3G). Because CTCF binding sites are enriched in the vicinity of the interactors (Figure 3H), it is possible that PARP1 dimers (Mendoza-Alvarez

(M) Normalized levels of expression (Table S4) of genes located within 10 kb from the interactors in hESCs and HEBs were color-coded in the network (zFPKM values are shown in the heatmap inset).

(N) Nearest neighbor analysis of active (within 10 kb from the interactor) versus inactive nodes (inactive genes as well as gene deserts).

(O) Assessment of the assortativity coefficient of the network nodes based on transcriptional potential. Perfect segregation of active and inactive interactors would result in an assortativity coefficient equal to +1, whereas negative values suggest disassortative mixing. The assortativity coefficient by transcriptional activity was  $-0.049$  and  $-0.046$  for the active/inactive category of hESCs and HEBs, respectively, indicating lack of segregation. See also Figure S1 and Tables S1, S2, S3, and S4.

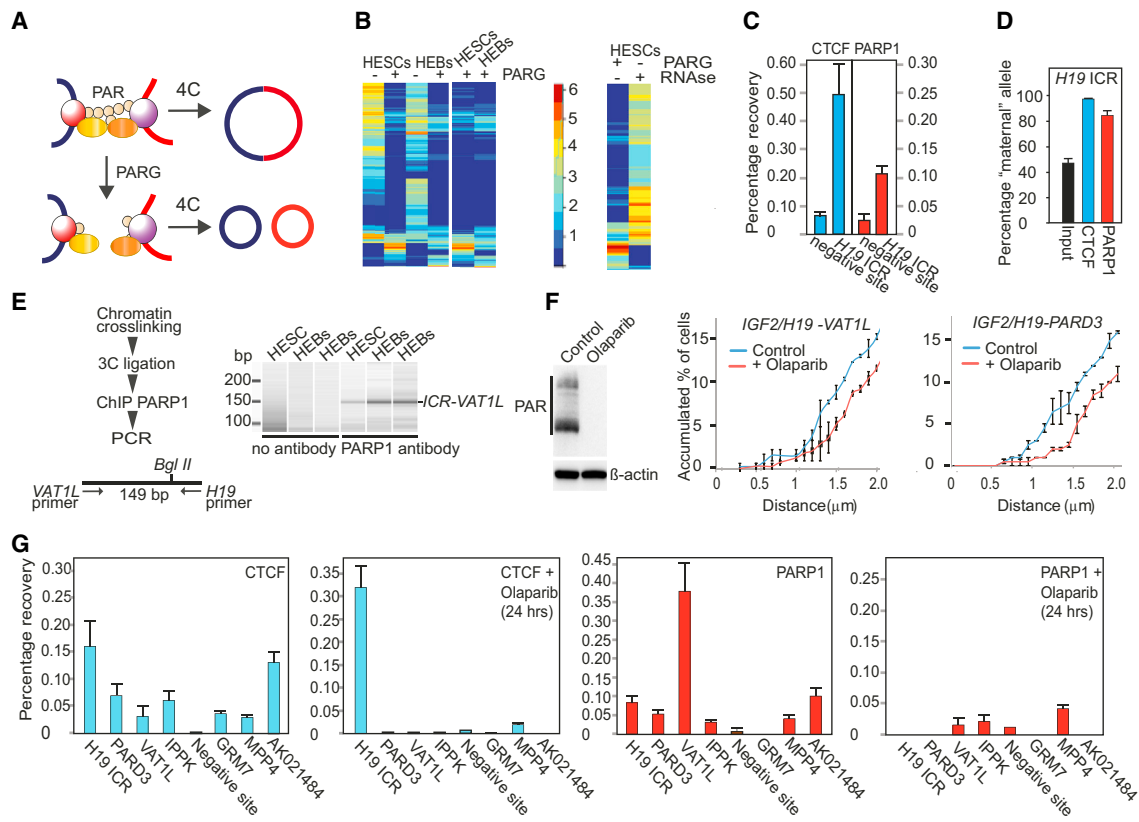


**Figure 2. Central Chromatin Hubs Are Occupied by CTCF and PARP1**

(A) Schematic of the presence of PAR in interacting chromatin fiber complexes.

(B) Heatmaps (in log<sub>2</sub>) comparing the H19 ICR interactome in control and PARG-treated hESCs or HEBs, highlighting the similarity of the interactomes remaining after PARG treatment in hESCs and HEBs. Right: comparison of the results of PARG and RNase treatments after formaldehyde crosslinking but before the DNA ligation step of the 4C analysis.

(C and D) ChIP analysis of PARP1 occupancy at the H19 ICR (C) and allele specificity (D). Data are represented as mean ± SEM.

(E) ChIP-loop analysis (a schematic is shown at the left) showing the presence of PARP1 in the H19 ICR-VAT1L complex (verified by sequencing; data not shown) in hESCs and HEBs (right). 3C, chromosome conformation capture.

(F) Left: western blot analysis of PAR levels in control and olaparib-treated hESCs. Center and right: the physical distances between IGF2/H19 and VAT1L or PARD3 in control and olaparib-treated (24 hr) hESCs by 3D DNA FISH. 200 alleles were counted in duplicate experiments. Data are represented as mean ± SEM. The statistical significance of the olaparib-induced change in proximities within the entire dataset was assessed by Kolmogorov-Smirnov (KS) test at a significance level of 0.05 ( $p \leq 0.05$  for IGF2/H19-VAT1L and  $p \leq 0.01$  for IGF2/H19-PARD3). A series of two-tailed Fisher's exact tests identified that the lowest calculated p values were at distances up to 2.6 μm ( $p \leq 0.01$ ) and up to 3.2 μm ( $p \leq 0.001$ ) for IGF2/H19-VAT1L and IGF2/H19-PARD3 proximities, respectively.

(G) ChIP analysis of CTCF and PARP1 binding at the H19 ICR and at its interactors in hESCs with or without 24 hr pre-treatment of hESCs with olaparib. CDC42EP3 served as a negative control (Experimental Procedures). Data are represented as mean ± SEM. p values for (C) and (G) are shown in Table S5. IPPK, inositol 1,3,4,5,6-pentakisphosphate 2-kinase.

See also Figure S2.

and Alvarez-Gonzalez, 1993) bridge two different CTCF binding sites (Figure 3I). Finally, PAR-protein interactions could further diversify the network (Figure 3J).

### PARP1 and CTCF Regulate Circadian Transcription by Promoting the Oscillating Recruitment of Circadian Loci to the Nuclear Periphery upon Serum Shock

The extensive communication between active genes and repressed domains within the network suggests that the interactome functions in the fine-tuning of transcription. Because PARP1 facilitates the entrainment of circadian rhythm to feeding (Asher et al., 2010), we performed permutation-based enrich-

ment analyses to score for the over-representation of active genes potentially under circadian control at different distances from the point of interaction in the 4C library from hESCs and hEBs (Table S6). Interestingly, circadian genes enriched in lipid metabolism were over-represented in the interactome, specifically at a 10-kb distance from the site of interaction (Figure 4A; Table S6), indicating that the interactors might act as cis-acting regulatory elements. Importantly, the circadian genes active in hESCs and hEBs (Table S4) displayed extensive interactions with repressed domains and constitutive LADs (Tables S6 and S7; Figure 4B, left right images of sub-networks impinging on the circadian node YAF2 or on a LAD). A nearest neighbor

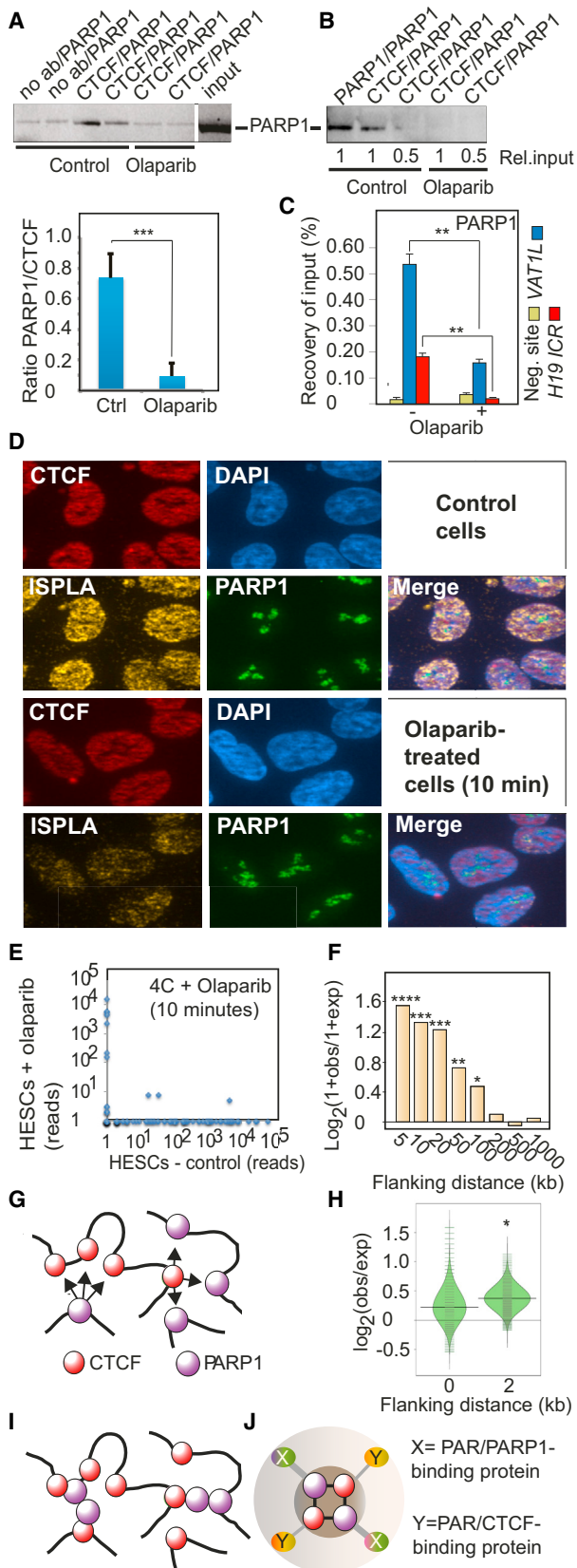


**Figure 3. CTCF-PARP1 Interactions Regulate the Assembly of the Inter-chromosomal Network**

(A) Co-immunoprecipitation of CTCF-PARP1 complexes from nuclear extracts in control (Ctrl) samples or samples exposed to short-term (2-hr) olaparib treatment (top). The white space indicates that the intervening lanes between the input sample and the rest of the gel were removed from the image. Quantitation of co-immunoprecipitation analyses of four different nuclear lysates derived from control and olaparib-treated cells is shown at the bottom. ab, antibody.

(B) Co-immunoprecipitation of CTCF-PARP1 complexes using recombinant proteins (at molar ratios of 1:1 and 0.5:1) in the absence or presence of 10-min olaparib treatment. Rel. input, relative input.

(C) ChIP analysis of PARP1 occupancy at the indicated sites in hESC chromatin, which was formaldehyde-crosslinked for 10 min in the presence or absence of olaparib. neg, negative.

(D) Effect of olaparib exposure during the formaldehyde crosslinking step on CTCF-PARP1 proximities as determined by ISPLA.

(E) Effect of 10-min olaparib treatment (during formaldehyde fixation) on the chromatin network, as determined by 4C using the *H19* ICR as bait.

(F) Permutation-based enrichment analyses of the percentage of overlap between regions (5–1000 kb) flanking the interactors of the *H19* ICR. Obs, observed; exp, expected.

(G) Model showing that chromatin interactomes can form as a result of stochastic movements and specific interactions between CTCF and PARP1-complexed chromatin hubs.

(H) CTCF binding sites are enriched within 2 kb of the site of the interaction in the *H19* ICR interactome.

(I) and (J) Distal CTCF binding sites might interact by promoting the formation of PARP1 dimers (I). The central core of the network might be diversified further by secondary interactions between PARylated PARP1/CTCF and PAR-binding factors (J).

Data are represented as mean  $\pm$  SEM. \*p  $\leq$  0.05, \*\*p  $\leq$  0.005, \*\*\*p  $\leq$  0.0005, \*\*\*\*p  $\leq$  0.0001. See also Figure S3.

analysis revealed that the percentage of interactions between circadian genes and LADs was higher than between circadian genes (Figure 4C). In agreement with the dynamic localization of LADs to the nuclear periphery (Figures 4D and 4E), 3D DNA FISH measured frequent proximities between the active *VAT1L* node and four different constitutive LADs at the nuclear envelope in hESCs (Figures 4D and 4F). Finally, reinforcing a role for PARP functions/protein interactome in the recruitment of circadian regions to LADs, olaparib reduced the proximity of the *IGF2/H19*, *TLK1*, and *PARD3* loci to the nuclear periphery in hESCs (Figure 4G).

Therefore, circadian regulation of transcription might involve the rhythmic recruitment of circadian loci to the repressive environment of the lamina to attenuate transcription in an oscillating manner. To explore this possibility, we used serum shock to synchronize cellular circadian rhythms in cultured cells (Balsalobre et al., 1998). Because the circadian rhythm of hESCs could not be synchronized (data not shown; Yagita et al., 2010) and the heterogeneous composition of hEBs (Experimental Procedures) compromised interpretation, we turned to HCT116 cells. These cells display circadian gene expression (Relógio et al., 2014) and significant amplitude in the oscillating transcription of a circadian chromatin hub of the 4C network, *PARD3*, upon serum shock (Figures S4A and S4B). Given the role of CTCF and PARP1 in the interactions between LADs and circadian genes, we first examined CTCF-PARP1 proximities during the circadian cycle. Using ISPLA in serum-shocked cells, we observed that CTCF-PARP1 interactions oscillated with peaks at 8 and 32 hr and

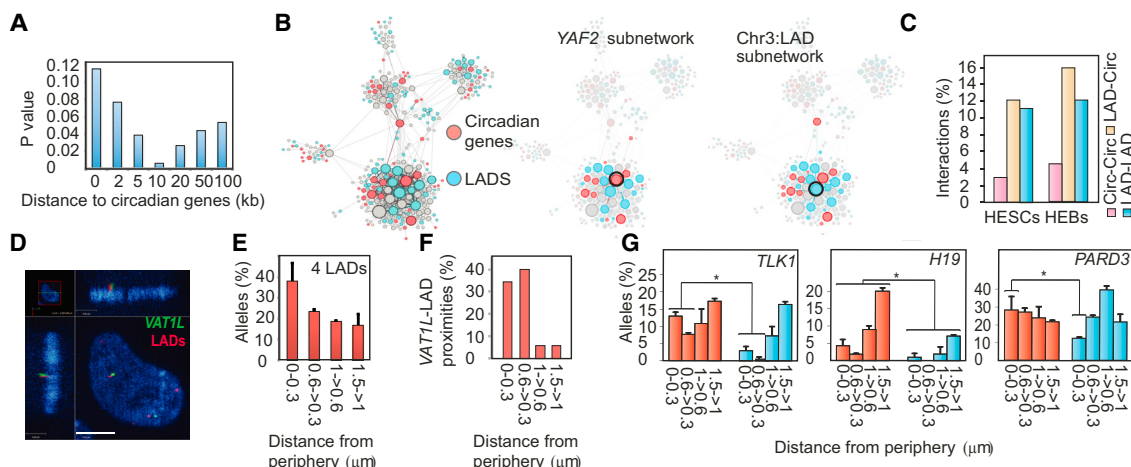


**Figure 4. The Network Structure Reflects Extensive Interactions between Active Genes under Circadian Control and LADs**

(A) Enrichment analyses of circadian genes in the *H19* ICR interactome at different distances from the site of interaction, using the mouse liver 48-hr dataset (Hughes et al., 2009).

(B) The distribution of LADs and transcriptionally active circadian genes (as measured by RNA-seq) in hESCs and hEBs within the network. The center and right images show sub-networks impinging on chromatin hubs (circled) mapping to an active circadian gene (*YAF2*) or LAD (chr3:5865326-5865515).

(C) Nearest neighbor analysis illustrates the frequency of interactions between LADs (LAD-LAD), between circadian genes and LADs (LAD-Circ), or between circadian genes (Circ-Circ). The assortativity coefficients for interactions between active circadian genes and LADs were -0.0097 in hESCs and -.004 in hEBs, indicating lack of segregation.

(D) Confocal DNA FISH image illustrating the proximity between two chromatin hubs (a LAD and *VAT1L*) at the nuclear periphery in hESCs. Scale bar, 4.5 μm.

(E) LADs dynamically localize to the nuclear periphery in hESCs.

(F) When *VAT1L* is proximal to a LAD, it is generally juxtaposed to the nuclear periphery.

(G) Olaparib counteracted the localization of three chromatin hubs to the nuclear periphery. 100 alleles were counted in duplicate experiments.

Data are represented as mean ± SEM. \*p < 0.05. See also Figure S4 and Tables S6 and S7.

with a phasing of approximately 24 hr (Figure 5A, quantified in Figure 5B; immunostaining of CTCF and PARP1 is shown in Figure S5). Strikingly, the proximity between these factors occurred primarily at the nuclear periphery (Figure 5C), whereas PARP1-PARP1 (Figure 5D) and CTCF-CTCF (Figure 5E) proximity showed different patterns.

To assess how oscillating formation CTCF-PARP1 complexes related to the potentially rhythmic recruitment of the bait and circadian network nodes to the lamina, the distance between circadian loci and the lamina (visualized by lamin A/C staining) was measured by 3D DNA FISH at the indicated time points (Figure 6A). Figure 6B illustrates that *IGF2/H19* co-localized with the lamina in rhythmic patterns, peaking at 0 and 24 hr following serum shock. Another chromatin hub, *VAT1L*, was similarly recruited to the lamina at 0 and 24 hr upon serum shock (Figure 6C). Strikingly, two other circadian chromatin hubs, *TARDBP* (TAR DNA binding protein, which regulates transcription and splicing) and *PARD3*, were recruited to the nuclear periphery with a different phasing, with the peak of recruitment shifted by approximately 8 hr (Figure 6C).

Because *H19/IGF2* and *VAT1L* displayed low transcriptional activity in HCT116 cells, whereas *PARD3* and *TARBD* were active (Figures 6D–6F), we examined whether inhibition of transcription would accelerate the recruitment of *TARDBP* and *PARD3* to the lamina. To this end, HCT116 cells were treated with Flavopiridol (Shannon et al., 2003) for 8 hr before harvesting the serum-shocked cells at either 0 or 8 hr. Interestingly, Flavopiridol not only inhibited transcription (Figures 6F and 6G) but

also accelerated the juxtaposition of *TARDBP* and *PARD3* to the lamina upon serum shock (Figure 6H).

Given the role of PARP1 and CTCF in the interactome between circadian loci and LADs, we examined the effects of olaparib and small interfering RNA (siRNA)-mediated downregulation of either CTCF or PARP1 on the recruitment of circadian loci to the lamina. Importantly, both pharmacological inhibition of PARP activity by olaparib (Figure 6I) and the absence of PARP1 protein (Figures 6J and 6L), or CTCF (Figures 6J and 6L) abolished the circadian recruitment of *IGF2/H19* and *PARD3* loci to the envelope. Furthermore, olaparib counteracted circadian *PARD3* mRNA accumulation upon serum shock in HCT116 cells (Figure S6A). Finally, both olaparib and downregulation of either CTCF or PARP1 counteracted serum shock-induced circadian oscillations in *PARD3* transcription, as measured by RNA FISH (Figures 6K and 6L; Figure S6B). Therefore, both CTCF and PARP1 levels as well as PARP activity/protein interactome played important roles in the recruitment of circadian loci to the nuclear periphery and the entrainment of circadian transcription.

Interestingly, the transcriptional activity of the *PARD3* gene remained high at the peak of its recruitment to the lamina (Figure 7A). Reasoning that repression was not immediate, we re-analyzed the kinetics of recruitment to the nuclear envelope and transcription with 2-hr intervals between 8 and 16 hr following serum shock. This approach revealed that transcriptional attenuation occurred between 10 and 12 hr (Figures 7B and 7C), following the peak of recruitment to the lamina at

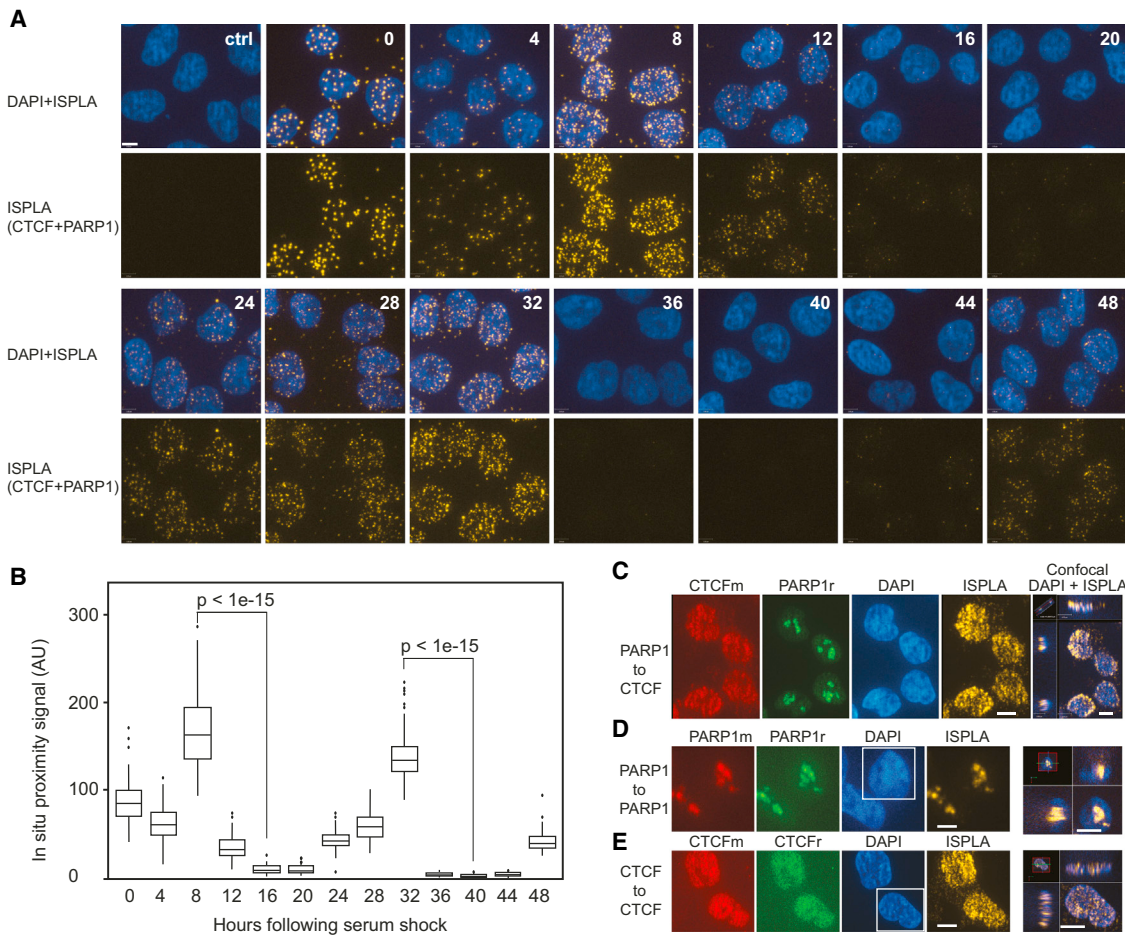


**Figure 5. Circadian Dynamics and Sub-nuclear Localization of CTCF-PARP1 Complex Formation**

(A) ISPLA of CTCF-PARP1 interactions during a 48-hr time period. Yellow dots depict in situ CTCF-PARP1 complexes counterstained by DAPI (blue).

(B) Quantification of ISPLA signals. Each data point represents 100 cells. Statistical significance was analyzed using two-tailed KS test. AU, arbitrary unit.

(C–E) Confocal images illustrate the localization of CTCF-PARP1 complexes at the nuclear periphery in HCT116 cells 8 hr following serum shock (C). For comparison, the distribution of PARP1-PARP1 (D) and CTCF-CTCF (E) ISPLA signals are shown in extended and confocal views (right). CTCFr/PARP1r and CTCFm/PARP1m depict rabbit and mouse primary antibodies, respectively. Scale bars, 6  $\mu$ m.

See also Figure S5.

10 hr (Figure 7D). The observation that at least one quarter of all *PARD3* alleles were juxtaposed to the nuclear periphery at any given time during a time period stretching from 0–12 hr, with a peak at 10 hr following serum shock, suggested that recruitment to the periphery preceded transcriptional attenuation by several hours. To examine this issue, the transcriptional activity of *PARD3* alleles located at the nuclear periphery was analyzed as above. Although *PARD3* was actively transcribed at the lamina at the time of the peak of its recruitment to the nuclear periphery, its activity was reduced markedly at this sub-compartment a few hours later, at 12 hr following serum shock (Figure 7E). We conclude that circadian recruitment of active *PARD3* alleles to the nuclear periphery preceded transcriptional attenuation.

Because repressive chromatin modifiers and H3K9me2 LOCKS (large organized chromatin enriched in lysine methylation) (Wen et al., 2009) are enriched at the lamina, we examined the presence of H3K9me2 at the *PARD3* locus in HCT116 cells.

ChIP sequencing (ChIP-seq) analysis documented enrichment in H3K9me2 but not in H3K27me3 at *PARD3* (Figure 7F). The presence of H3K9me2 at individual *PARD3* alleles was further explored in single cells by chromatin in situ proximity analysis (ChISP) (Chen et al., 2014a, 2014b; Figure 7G). ChISP translates the proximity between the H3K9me2 epitope and the epitopes generated by DNA FISH probes hybridizing to *PARD3* into a fluorescent signal, allowing the detection of chromatin modifications at individual *PARD3* alleles in the 3D context of the nucleus. Figure 7H shows that the presence of the repressive H3K9me2 at the *PARD3* locus was highest at the time of transcriptional attenuation and following the peak of its recruitment to the nuclear periphery. Furthermore, lower levels of this mark coincided with increased transcriptional activity in the nuclear interior (Figure 7H). The role of the oscillating acquisition of H3K9me2 in circadian transcription was further reinforced by the observation that depletion of H3K9me2 by inhibiting the enzymatic activity of G9a/Glp by

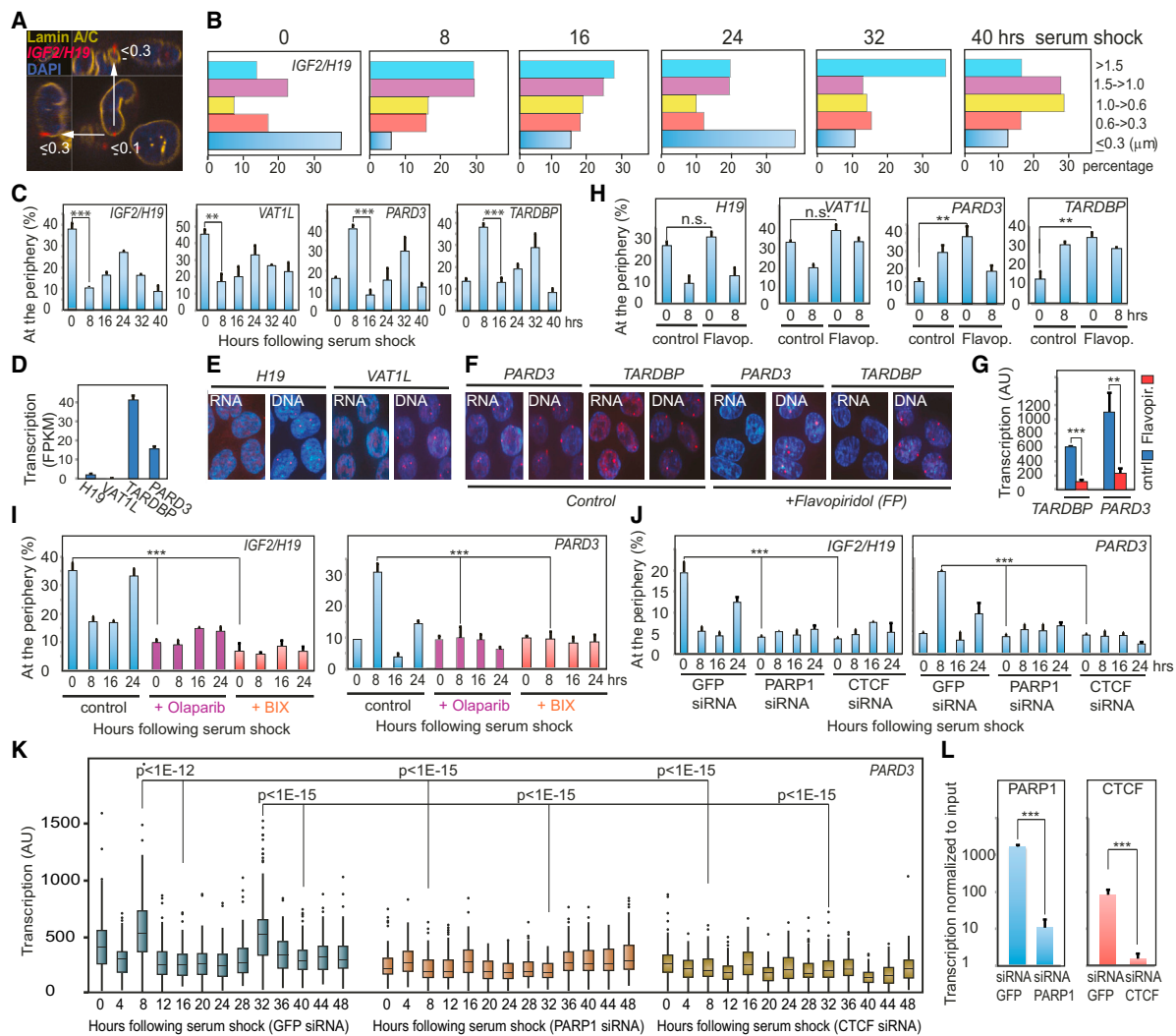


**Figure 6. PARP1 and CTCF Regulate the Recruitment of Clock-Controlled Chromatin Hubs to the Nuclear Periphery as well as Oscillating Transcription**

(A) Lamin A/C staining was combined with 3D DNA FISH to measure the physical distance between circadian loci and the lamina in HCT116 cells.

(B) Circadian recruitment of the *IGF2/H19* locus to the lamina was analyzed in HCT116 cells (as described in A) at the indicated time points upon serum shock.

(C) The circadian recruitment of *IGF2/H19*, *VAT1L*, *PARD3*, and *TARDBP* loci to the lamina, as measured by 3D DNA FISH and Lamin A/C staining (distance to lamina  $\leq 0.3\mu$ m).

(D) Analysis of transcription at four chromatin hubs in HCT116 cells by RNA-seq.

(E) RNA FISH analysis of *VAT1L* and *H19* transcription.

(F and G) RNA FISH analysis of *PARD3* or *TARDBP* (the probe also covered four neighboring circadian genes, including *MTORC*) transcription in the absence or presence of Flavopiridol (F). Quantitation of the results is shown in (G).

(H) Flavopiridol affected the timing of recruitment of *PARD3* and *TARDBP* but not that of the inactive *IGF2/H19* and *VAT1L* to the lamina in HCT116 cells.

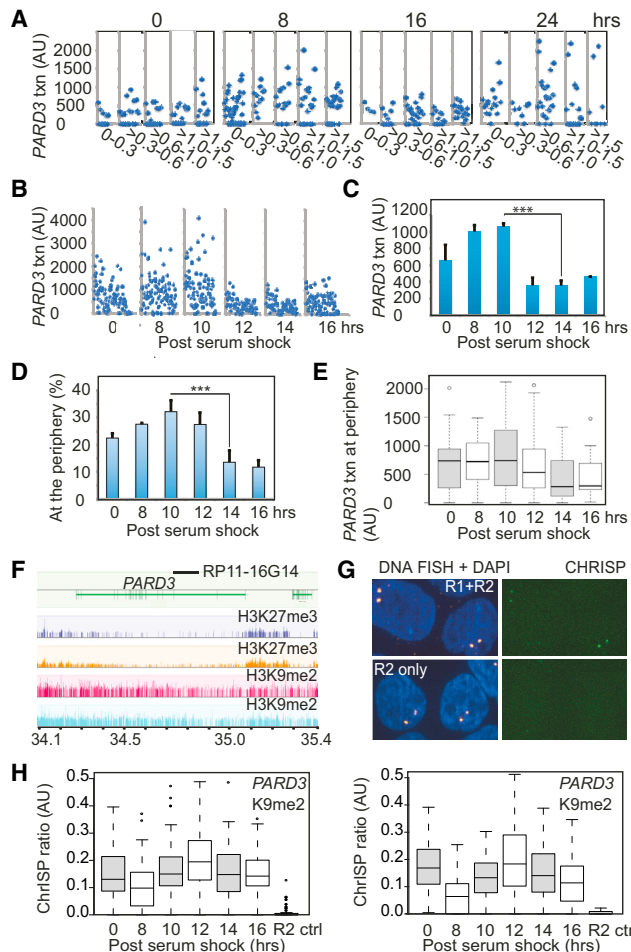
(I) Olaparib and BIX01294 antagonized the rhythmic juxtaposition of *IGF2/H19* and *PARD3* to the lamina. BIX, BIX01294.

(J) 3D DNA FISH analysis of proximity between the nuclear periphery and *IGF2/H19* or *PARD3* in HCT116 cells transfected with siRNA against GFP (control), PARP1, or CTCF transcripts.

(K) RNA FISH analysis of nuclear transcription at individual *PARD3* alleles during the circadian cycle in HCT116 cells transfected with siRNA against GFP, PARP1, or CTCF transcripts. Statistical significance was analyzed by two-tailed KS test (Supplemental Experimental Procedures). 60 cells were counted at each time point.

(L) Efficiency of siRNA-mediated downregulation of PARP1 and CTCF.

Each data point represents 150 alleles. Data are represented as mean  $\pm$  SEM. \* $p \leq 0.05$ , \*\* $p \leq 0.005$ , \*\*\* $p \leq 0.0005$ , \*\*\*\* $p \leq 0.0001$ ; Student's t test. n.s., not significant (indicates  $p > 0.05$ ). (Error bars represent mean  $\pm$  SEM). See also Figure S6.



- I
1. CTCF-PARP1 promote chromatin recruitment to the nuclear periphery  
2. Antagonism between CTCF-PARP1 and transcriptional elongation affects the timing of recruitment to the nuclear periphery  
3. Transcription is active all the way to the nuclear periphery  
4. Acquisition of repressive marks (H3K9me2) at the nuclear periphery  
5. Inactivated chromatin released from the nuclear periphery  
6. The attenuated state is gradually eroded to enable the next round of activation  
7. Transcriptional activation

**Figure 7. Transcriptional Attenuation of the *PARD3* gene Correlates with the Acquisition of H3K9me2 at the Lamina**

(A–D) Transcriptional activity of *PARD3* was measured by RNA FISH in relationship to the nuclear periphery upon serum shock. A detailed time course

BIX01294 (Kubicek et al., 2007; Chen et al., 2014b) abolished the recruitment of *PARD3* to the nuclear periphery (Figure 6l) and inhibited circadian oscillations in its transcription without affecting the mean level of transcription (Figures S6B–S6D). Taken together, the data are consistent with the notion that juxtaposition of *PARD3* to the nuclear periphery led to the time-dependent acquisition of H3K9me2 and circadian transcriptional attenuation.

## DISCUSSION

Our findings uncover an inter-chromosomal interactome organized by PARP1 and CTCF in hESCs and hEBs. The topology of the network shows extensive interactions between circadian genes and LADs at the nuclear periphery. Moreover, synchronization of the circadian rhythm in HCT116 cells by serum shock induces the coordinated oscillating recruitment of circadian loci to the nuclear envelope in a CTCF- and PARP1-dependent manner. Recruitment to the lamina is followed by the acquisition of H3K9me2 marks concomitant with transcriptional attenuation, highlighting a role for the chromatin environment at the nuclear envelope in the circadian attenuation of transcription.

### PARP1 and CTCF Organize an Inter-chromosomal Chromatin Fiber Interactome

The earlier observation that PARylation of CTCF is essential for its insulator function in *cis* (Yu et al., 2004) implies that dynamic interactions between chromatin hubs might primarily involve PARylated CTCF. The findings presented here illustrate, however, that protein-protein interactions between CTCF and PARP1 are indispensable for the formation of the *H19* interactome. Therefore, PARP1 is present in the interacting chromatin complexes (Figure 2E), and disruption of CTCF-PARP1 binding by 10-min incubation with olaparib disassembles the

analysis was performed to assess nuclear transcription of *PARD3* (B and C) and its recruitment to the lamina (D) by RNA and DNA FISH.

(E) Time-dependent decline in the transcriptional activity of *PARD3* at the lamina (distance from lamina  $\leq 0.3 \mu\text{m}$ ). 150 alleles were counted for each data point. Error bars indicate mean  $\pm$  SEM. \*\*\* $p < 0.0005$ , Student's t test.  
(F) ChIP-seq map of H3K9me2 and H3K27me3 at the *PARD3* locus in HCT116 cells. The numbers are in million base pairs (hg19).

(G) ChIPSP analysis of the presence of H3K9me2 at *PARD3* alleles. The R2 negative control illustrates that using only one antibody does not result in a background fluorescent signal.

(H) Two ChIPSP experiments (\*\*\* $p \leq 0.0005$ ) represented by box plots measuring the presence of the H3K9me2 at *PARD3* (160 alleles were counted for each time point in both experiments) in response to serum shock.

(I) Model explaining the oscillating recruitment of circadian loci to the nuclear periphery and subsequent transcriptional attenuation. Although CTCF-PARP1 complexes promote recruitment to the periphery, this process is delayed by transcriptional elongation. Active and inactive loci therefore reach the periphery at different time points upon serum shock. Recruitment of circadian loci to the lamina is followed by the acquisition of repressive H3K9me2 marks and gradual transcriptional attenuation at the lamina. Inactivated circadian loci are released from the lamina concomitant with the loss of CTCF-PARP1 interactions. The black-to-gray transition in "Transcription" indicates attenuated transcription. The arrows indicate forces regulating the recruitment of chromatin hubs to the nuclear periphery.

See also Figure S7.

interactome (Figure 3E). Furthermore, PAR is much more prevalent on PARP1 than on CTCF (Figures S2J and S2K). Accordingly, PARylation is much more prevalent at the *VAT1L* chromatin hub, showing prominent PARP1 binding (Figure S3B). Therefore, if PAR provides a surface for interactions to diversify the interactome, then it is most likely via PARylated PARP1 (Figure 3G). The interactome uncovered here is therefore distinct from the CTCF-PAR regulated intra-chromosomal network reported in *Drosophila* (Ong et al., 2013).

Interestingly, many of the reproducible hubs map to LADs and form a network with active transcriptional units. Because most of the proximities between *VAT1L* and LADs take place at the nuclear periphery (Figure 4F), we hypothesize that much of the chromatin fiber network is established at this compartment. This idea is further supported by the fact that four additional chromatin hubs were frequently positioned at the nuclear periphery in hESCs. These features likely depend on PARP1 activity/protein interactome because olaparib antagonizes both the proximity between interacting chromatin hubs and their localization to the nuclear periphery (Figures 4D–4G). In addition, olaparib affects the relative positions of *IGF2/H19* and *VAT1L* to their chromosome territories (Figures S1P and S1Q). We argue, therefore, that CTCF-PARP1 interactions not only organize interactions but also regulate chromatin mobility to increase the likelihood for encounters between loci located on different chromosomes and in different sub-nuclear compartments.

### Oscillating Interactions between Circadian Genes and LADs at the Lamina Promote Circadian Transcriptional Attenuation

The interactions between repressed and active regions in the 4C network differ from previous interactomes generated by the Hi-C method. Global maps of interaction frequencies have documented that repressed and active domains segregate in different sub-compartments of the nucleus (Bickmore and van Steensel, 2013; Dekker et al., 2013). However, the reproducible interactome between repressed LADs and active circadian loci in the network impinging on the *H19* ICR has led to the idea that this fraction of the network forms as a result of oscillating re-positioning of circadian loci to the lamina. Because this nuclear sub-compartment is enriched in repressive chromatin modifiers (Luperchio et al., 2014) that act in concert with members of the negative limb of circadian regulation (Duong and Weitz, 2014; Kim et al., 2014), we envisage that recruitment to the lamina contributes to circadian transcriptional attenuation.

In line with this, synchronization of the circadian rhythm in colon cancer cells by serum shock coordinates the circadian recruitment of clock-controlled loci to the envelope, followed by the acquisition of repressive chromatin marks concomitant with gradual transcriptional attenuation at the lamina (Figure 7I). Interestingly, not only active but also inactive loci undergo circadian recruitment to the lamina, albeit with peaks at different time points, suggesting the existence of a memory of circadian identity in the absence of transcription. Furthermore, the timing of recruitment can be altered by Flavopiridol, an inhibitor of transcriptional elongation, suggesting that histone modifications

deposited during elongation (Li et al., 2007) or changes in the level of torsional stress (Teves and Henikoff, 2014) might play roles in this process.

The circadian system uncovered here is likely to be intertwined with the central clock machinery. Indeed, *PER1* has also been recruited to the lamina similarly as the other clock-controlled genes (Figure S7). Moreover, its expression increases following its release from the lamina (Figure S7). The eventual encounter with the repressive chromatin environment at the nuclear periphery might therefore be essential for chromatin transitions from the positive to the negative limb of circadian regulation.

Importantly, these processes are regulated by PARP1 and CTCF, the latter being a housekeeping gene not previously associated with circadian mechanisms. Our findings demonstrate that PARP1 and CTCF interact with each other in a circadian manner, organize dynamic chromatin fiber interactions between circadian loci and LADs, and regulate the oscillating recruitment of circadian loci to the lamina to promote circadian oscillations in transcription upon serum shock. The sensitivity of these processes to disruption of CTCF-PARP1 interactions and PARP1 or CTCF downregulation advances our understanding of the complex role of PARP1 in the entrainment of the circadian system to feeding (Asher et al., 2010). PARP1 has been shown to modulate the binding kinetics of the CLOCK-BMAL1 complex to DNA (Asher et al., 2010) and the temporal interactions between members of the positive and negative limbs (Asher et al., 2010) to potentially coordinate transcriptional attenuation. Our data are consistent with the notion that PARP1 impacts the transition from the positive limb to the negative limb of the circadian cycle by also promoting the synchronized recruitment of active circadian genes to the repressive nuclear envelope. Therefore, the time-dependent steps of peripheral recruitment and the ensuing gradual attenuation of transcription likely contribute to the poorly understood principle of time delays in circadian regulation.

Although the mechanism underlying the release of circadian loci from the periphery is not addressed here, we predict that dissociation of CTCF-PARP1 complexes likely plays a role in this process. Because autoPARylation of PARP1 is known to evict PARP1 from chromatin, we predict that factors under circadian control might influence the rhythmic stability of the CTCF-PARP1 complexes by affecting PARP1 activity (Bellet et al., 2011).

In summary, we demonstrated that circadian regulation of transcription involves the rhythmic recruitment of circadian genes to the repressive environment of the nuclear periphery. Apart from documenting a pivotal role of the nuclear architecture in circadian control, our observations also suggest that the time delay between transcriptional activation and attenuation during the circadian cycle involves the timed removal of circadian genes from nuclear sub-compartments permissible for transcription. Collectively, these observations provide a plausible explanation for the absence of circadian rhythm in hESCs because these cells lack large domains of repressive chromatin structures at the nuclear periphery (Wen et al., 2009). Epimutations of such domains (Wen et al., 2009) are therefore predicted to antagonize circadian regulation to disconnect metabolic states from core

cellular functions in complex diseases such as cancer and diabetes.

## EXPERIMENTAL PROCEDURES

### Cell Cultures

Female hESCs (HS181) were maintained on irradiated male feeder fibroblasts, and HEBs were generated as described previously (Imreh et al., 2004). The contamination of feeders in hESCs/HEBs was  $1.05\% \pm 0.03\%$  and  $0.07\% \pm 0.06\%$ , respectively, as determined by qPCR (Supplemental Experimental Procedures). Immunofluorescence analysis determined that the EBs contained 8% mesodermal (vimentin), 43% endodermal (GATA4), and 49% neuro-ectodermal (nestin) lineages. HCT116 cells were maintained as described previously (Chen et al., 2014a). Olaparib (0.3  $\mu$ M final concentration) and Flavopiridol (2  $\mu$ M final concentration) treatments were performed as indicated in the text. Serum shock treatments were performed as described previously (Balsalobre et al., 1998), and cells were retrieved at the time points indicated in the text.

### RNA/DNA FISH Analysis

Sonicated bacterial artificial chromosomes/clones (BACs) (Supplemental Experimental Procedures) were labeled with Cy3-dCTP, Cy5-dCTP, Green-dUTP, Aqua-dUTP (catalog nos. 02N32-050 and 02N35-050, Abbott Molecular), digoxigenin-11-dUTP (catalog no. 11209256910, Roche Applied Science), or ChromaTide Texas red-12-dUTP (catalog no. C-7631, Invitrogen) using the Bioprime array comparative genomic hybridization (CGH) kit (catalog no. 18095-011, Invitrogen). Cells were grown on Lab-Tek II chamber slides and crosslinked with 3% paraformaldehyde (PFA) in the presence of 4 mM vanadyl-ribonucleoside complex at room temperature (RT). After crosslinking, cells were permeabilized with 0.5% Triton X-100 in 2 $\times$  sodium salt citrate (SSC) for 10 min at RT. Genomic DNA was denatured in 2 $\times$  SSC/90% formamide at 80°C for 30 min. The labeled probes mixed with unlabeled Cot-1 DNA (catalog no. 15279-011, Invitrogen, 100 ng/ $\mu$ l) were hybridized overnight at 37°C in hybridization buffer (2 $\times$  SSC, 50% formamide, and 12% dextran sulfate). Samples were washed twice with 2 $\times$  SSC/50% formamide for 15 min each at 42°C and twice with 2 $\times$  SSC for 15 min each at 42°C, followed by an overnight wash in PBS at 4°C. Finally, slides were mounted in Vectashield (H1200, Vector Laboratories) with 4',6-diamidino-2-phenylindole (DAPI). RNA FISH was performed as above, but the denaturation step was omitted. Cell imaging and generation of optical sections in three dimensions was carried out on a Leica DMI 3000B fluorescence microscope with an Opti-Grid device using Velocity software (PerkinElmer). 200 nuclei were counted for each instance. The center of each FISH signal was selected, and the x, y, and z coordinates were recorded for distance calculation. The percentage of cells having two signals in defined distance bins was calculated, and the cumulative distribution was plotted.

### 4C

Formaldehyde crosslinking of hESCs and hEBs was performed as described previously (Göndör et al., 2008) in the presence of 4 mM (final concentration) vanadyl-ribonucleoside complex (S1402S, New England Biolabs). Chromatin representing  $10^6$  formaldehyde-fixed hESCs or EB cells was digested with BgIII for 2 weeks at 37°C in the presence of 1 U/ $\mu$ l RNasin Plus (Promega). 4C was performed as described previously (Göndör et al., 2008). PAR was removed by incubating the crosslinked chromatin with 25 ng/ml (final concentration) recombinant PARG (catalog no. 4680-096-01, Trevigen) in the presence of 2 mM (final concentration) DTT in BgIII restriction buffer at 25°C prior to BgIII digestion for 24 hr, followed by a further incubation for 2 weeks at 37°C parallel to restriction enzyme digestion. For the generation of RNase-treated samples, cross-linked chromatin was incubated with RNase A (0.8 mg/ml final concentration) during the period of restriction enzyme digestion. Following intra-molecular ligation, reversal of crosslink and DNA purification were performed as described previously (Göndör et al., 2008). All primers used to amplify the 4C material are listed in the Supplemental Experimental Procedures.

All other methods can be found in the Supplemental Experimental Procedures.

## ACCESSION NUMBERS

The accession number for the 4C-seq and RNA-seq data reported in this paper is GEO: GSE26880. The accession number for the ChIP-seq data reported in this paper is GEO: GSE58534.

## SUPPLEMENTAL INFORMATION

Supplemental Information includes Supplemental Experimental Procedures, seven figures, and seven tables and can be found with this article online at <http://dx.doi.org/10.1016/j.molcel.2015.07.019>.

## AUTHOR CONTRIBUTIONS

H.Z. performed the RNA/DNA FISH, siRNA transfection, and ISPLA analyses. E.G.S. designed and implemented the majority of computational/statistical analyses, performed the network integrative analyses, and mapped and processed the RNA-seq data. N.S. performed all ChIP analyses and contributed to the 4C analyses. L.M.A. conducted the co-IP, ChIPSP, and RNA FISH analyses. B.A.S. performed the RNA/DNA FISH analyses. J.P.S. mapped 4C-seq data and assisted with the computational/statistical analyses. X.C., A.L.R., C.S., F.S., and B.N. conducted the DNA FISH analyses. X.C. also assisted with siRNA transfection experiments. C.D.M.d.L. implemented the qPCR analyses of circadian rhythms, and A.L.R. performed the PARP1 immunostaining of hESCs. O.L. and T.H. performed the CTCF-PARP1 activation analyses. S.Y. performed the PAR immunostaining analyses of hESCs. M.I. developed the allele-specific qPCR analysis. L.S.R. assisted with the identification of *ICR-VAT1L*-PARP1 complexes. E.F. conceived the permutation-based enrichment analysis and assisted with the computational/statistical analyses. M.P.I. provided hESCs and HEBs. A.G. designed the experiments, performed the 3C/4C and ChIP-loop experiments, contributed to the co-IP experiments, and wrote the manuscript.

## ACKNOWLEDGMENTS

We gratefully acknowledge assistance from Alejandro Fernandez-Woodbridge with mapping the 4C-seq. We also acknowledge the ENCODE Consortium and the University of Texas at Austin for generating the H1-HESC CTCF binding sites dataset. This work was supported by the Swedish Science Research Council (VR-99X-21992-01-03, VR-M2579, and VR-NT4448), the Swedish Pediatric Cancer Foundation, the Swedish Cancer Foundation (CAN2012/23), the Lundberg Foundation, Karolinska Institutet, and the KA Wallenberg Foundation.

Received: January 16, 2015

Revised: May 20, 2015

Accepted: July 21, 2015

Published: August 27, 2015

## REFERENCES

- Aguilar-Arnal, L., Hakim, O., Patel, V.R., Baldi, P., Hager, G.L., and Sassone-Corsi, P. (2013). Cycles in spatial and temporal chromosomal organization driven by the circadian clock. *Nat. Struct. Mol. Biol.* 20, 1206–1213.
- Asher, G., and Schibler, U. (2011). Crosstalk between components of circadian and metabolic cycles in mammals. *Cell Metab.* 13, 125–137.
- Asher, G., Reinke, H., Altmeyer, M., Gutierrez-Arcelus, M., Hottiger, M.O., and Schibler, U. (2010). Poly(ADP-ribose) polymerase 1 participates in the phase entrainment of circadian clocks to feeding. *Cell* 142, 943–953.
- Balsalobre, A., Damiola, F., and Schibler, U. (1998). A serum shock induces circadian gene expression in mammalian tissue culture cells. *Cell* 93, 929–937.
- Becker, K.G., Barnes, K.C., Bright, T.J., and Wang, S.A. (2004). The genetic association database. *Nat. Genet.* 36, 431–432.

- Bellet, M.M., Orozco-Solis, R., Sahar, S., Eckel-Mahan, K., and Sassone-Corsi, P. (2011). The time of metabolism: NAD<sup>+</sup>, SIRT1, and the circadian clock. *Cold Spring Harb. Symp. Quant. Biol.* 76, 31–38.
- Beneke, S. (2012). Regulation of chromatin structure by poly(ADP-ribosylation). *Front. Genet.* 3, 169.
- Bickmore, W.A., and van Steensel, B. (2013). Genome architecture: domain organization of interphase chromosomes. *Cell* 152, 1270–1284.
- Chen, X., Shi, C., Yammie, S., Göndör, A., Rönnlund, D., Fernandez-Woodbridge, A., Sumida, N., Widengren, J., and Ohlsson, R. (2014a). Chromatin *in situ* proximity (ChIPSP): single-cell analysis of chromatin proximities at a high resolution. *Biotechniques* 56, 117–118, 120–124.
- Chen, X., Yammie, S., Shi, C., Tark-Dame, M., Göndör, A., and Ohlsson, R. (2014b). The visualization of large organized chromatin domains enriched in the H3K9me2 mark within a single chromosome in a single cell. *Epigenetics* 9, 1439–1445.
- Cho, H., Zhao, X., Hatori, M., Yu, R.T., Barish, G.D., Lam, M.T., Chong, L.W., DiTacchio, L., Atkins, A.R., Glass, C.K., et al. (2012). Regulation of circadian behaviour and metabolism by REV-ERB- $\alpha$  and REV-ERB- $\beta$ . *Nature* 485, 123–127.
- Dekker, J., Marti-Renom, M.A., and Mirny, L.A. (2013). Exploring the three-dimensional organization of genomes: interpreting chromatin interaction data. *Nat. Rev. Genet.* 14, 390–403.
- Duong, H.A., and Weitz, C.J. (2014). Temporal orchestration of repressive chromatin modifiers by circadian clock Period complexes. *Nat. Struct. Mol. Biol.* 21, 126–132.
- Ernst, J., Kheradpour, P., Mikkelsen, T.S., Shores, N., Ward, L.D., Epstein, C.B., Zhang, X., Wang, L., Issner, R., Coyne, M., et al. (2011). Mapping and analysis of chromatin state dynamics in nine human cell types. *Nature* 473, 43–49.
- Göndör, A., and Ohlsson, R. (2009). Chromosome crosstalk in three dimensions. *Nature* 461, 212–217.
- Göndör, A., Rougier, C., and Ohlsson, R. (2008). High-resolution circular chromosome conformation capture assay. *Nat. Protoc.* 3, 303–313.
- Guastafiero, T., Cecchinelli, B., Zampieri, M., Reale, A., Riggio, G., Sthandler, O., Zupi, G., Calabrese, L., and Caiafa, P. (2008). CCCTC-binding factor activates PARP-1 affecting DNA methylation machinery. *J. Biol. Chem.* 283, 21873–21880.
- Guelen, L., Pagie, L., Brasset, E., Meuleman, W., Faza, M.B., Talhout, W., Eussen, B.H., de Klein, A., Wessels, L., de Laat, W., and van Steensel, B. (2008). Domain organization of human chromosomes revealed by mapping of nuclear lamina interactions. *Nature* 453, 948–951.
- Hughes, M.E., DiTacchio, L., Hayes, K.R., Vollmers, C., Pulivarthy, S., Baggs, J.E., Panda, S., and Hogenesch, J.B. (2009). Harmonics of circadian gene transcription in mammals. *PLoS Genet.* 5, e1000442.
- Imreh, M.P., Wolbank, S., Unger, C., Gertow, K., Aints, A., Szeles, A., Imreh, S., Hovatta, O., Fried, G., Dilber, S., and Ahrlund-Richter, L. (2004). Culture and expansion of the human embryonic stem cell line HS181, evaluated in a double-color system. *Stem Cells Dev.* 13, 337–343.
- Janich, P., Pascual, G., Merlos-Suárez, A., Batlle, E., Ripperger, J., Albrecht, U., Cheng, H.Y., Obrietan, K., Di Croce, L., and Benitah, S.A. (2011). The circadian molecular clock creates epidermal stem cell heterogeneity. *Nature* 480, 209–214.
- Kim, J.Y., Kwak, P.B., and Weitz, C.J. (2014). Specificity in circadian clock feedback from targeted reconstitution of the NuRD corepressor. *Mol. Cell* 56, 738–748.
- Krishnakumar, R., and Kraus, W.L. (2010). The PARP side of the nucleus: molecular actions, physiological outcomes, and clinical targets. *Mol. Cell* 39, 8–24.
- Kubicek, S., O'Sullivan, R.J., August, E.M., Hickey, E.R., Zhang, Q., Teodoro, M.L., Rea, S., Mechta, K., Kowalski, J.A., Homon, C.A., et al. (2007). Reversal of H3K9me2 by a small-molecule inhibitor for the G9a histone methyltransferase. *Mol. Cell* 25, 473–481.
- Li, B., Carey, M., and Workman, J.L. (2007). The role of chromatin during transcription. *Cell* 128, 707–719.
- Luperchio, T.R., Wong, X., and Reddy, K.L. (2014). Genome regulation at the peripheral zone: lamina associated domains in development and disease. *Curr. Opin. Genet. Dev.* 25, 50–61.
- Mendoza-Alvarez, H., and Alvarez-Gonzalez, R. (1993). Poly(ADP-ribose) polymerase is a catalytic dimer and the automodification reaction is intermolecular. *J. Biol. Chem.* 268, 22575–22580.
- Nagano, T., Lubling, Y., Stevens, T.J., Schoenfelder, S., Yaffe, E., Dean, W., Laue, E.D., Tanay, A., and Fraser, P. (2013). Single-cell Hi-C reveals cell-to-cell variability in chromosome structure. *Nature* 502, 59–64.
- Ohlsson, R., Lobanenkov, V., and Klenova, E. (2010). Does CTCF mediate between nuclear organization and gene expression? *BioEssays* 32, 37–50.
- Ong, C.T., and Corces, V.G. (2014). CTCF: an architectural protein bridging genome topology and function. *Nat. Rev. Genet.* 15, 234–246.
- Ong, C.T., Van Bortle, K., Ramos, E., and Corces, V.G. (2013). Poly(ADP-ribosylation) regulates insulator function and intrachromosomal interactions in *Drosophila*. *Cell* 155, 148–159.
- Pettitt, S.J., Rehman, F.L., Bajrami, I., Brough, R., Wallberg, F., Kozarewa, I., Fenwick, K., Assiotis, I., Chen, L., Campbell, J., et al. (2013). A genetic screen using the PiggyBac transposon in haploid cells identifies Parp1 as a mediator of olaparib toxicity. *PLoS ONE* 8, e61520.
- Reddy, K.L., and Feinberg, A.P. (2013). Higher order chromatin organization in cancer. *Semin. Cancer Biol.* 23, 109–115.
- Relogio, A., Thomas, P., Medina-Pérez, P., Reischl, S., Bervoets, S., Gloc, E., Riemer, P., Mang-Fatehi, S., Maier, B., Schäfer, R., et al. (2014). Ras-mediated deregulation of the circadian clock in cancer. *PLoS Genet.* 10, e1004338.
- Sahar, S., and Sassone-Corsi, P. (2012). Regulation of metabolism: the circadian clock dictates the time. *Trends Endocrinol. Metab.* 23, 1–8.
- Schoenfelder, S., Sexton, T., Chakalova, L., Cope, N.F., Horton, A., Andrews, S., Kurukuti, S., Mitchell, J.A., Umlauf, D., Dimitrova, D.S., et al. (2010). Preferential associations between co-regulated genes reveal a transcriptional interactome in erythroid cells. *Nat. Genet.* 42, 53–61.
- Shannon, P., Markiel, A., Ozier, O., Baliga, N.S., Wang, J.T., Ramage, D., Amin, N., Schwikowski, B., and Ideker, T. (2003). Cytoscape: a software environment for integrated models of biomolecular interaction networks. *Genome Res.* 13, 2498–2504.
- Shi, S.Q., Ansari, T.S., McGuinness, O.P., Wasserman, D.H., and Johnson, C.H. (2013). Circadian disruption leads to insulin resistance and obesity. *Curr. Biol.* 23, 372–381.
- Takahashi, J.S., Hong, H.K., Ko, C.H., and McDearmon, E.L. (2008). The genetics of mammalian circadian order and disorder: implications for physiology and disease. *Nat. Rev. Genet.* 9, 764–775.
- Tallis, M., Morra, R., Barkauskaite, E., and Ahel, I. (2014). Poly(ADP-ribosylation) in regulation of chromatin structure and the DNA damage response. *Chromosoma* 123, 79–90.
- Teves, S.S., and Henikoff, S. (2014). DNA torsion as a feedback mediator of transcription and chromatin dynamics. *Nucleus* 5, 211–218.
- Towbin, B.D., González-Aguilera, C., Sack, R., Gaidatzis, D., Kalck, V., Meister, P., Askjaer, P., and Gasser, S.M. (2012). Step-wise methylation of histone H3K9 positions heterochromatin at the nuclear periphery. *Cell* 150, 934–947.
- Wen, B., Wu, H., Shinkai, Y., Irizarry, R.A., and Feinberg, A.P. (2009). Large histone H3 lysine 9 dimethylated chromatin blocks distinguish differentiated from embryonic stem cells. *Nat. Genet.* 41, 246–250.
- Xu, M., and Cook, P.R. (2008). Similar active genes cluster in specialized transcription factories. *J. Cell Biol.* 181, 615–623.
- Yagita, K., Horie, K., Koinuma, S., Nakamura, W., Yamanaka, I., Urasaki, A., Shigeyoshi, Y., Kawakami, K., Shimada, S., Takeda, J., and Uchiyama, Y. (2010). Development of the circadian oscillator during differentiation of mouse embryonic stem cells *in vitro*. *Proc. Natl. Acad. Sci. USA* 107, 3846–3851.
- Yu, W., Ginjala, V., Pant, V., Chernukhin, I., Whitehead, J., Docquier, F., Farrar, D., Tavoosidana, G., Mukhopadhyay, R., Kanduri, C., et al. (2004).

- Poly(ADP-ribosylation) regulates CTCF-dependent chromatin insulation. *Nat. Genet.* 36, 1105–1110.
- Zhang, E.E., and Kay, S.A. (2010). Clocks not winding down: unravelling circadian networks. *Nat. Rev. Mol. Cell Biol.* 11, 764–776.
- Zhao, Z., Tavoosidana, G., Sjölander, M., Göndör, A., Mariano, P., Wang, S., Kanduri, C., Lezcano, M., Sandhu, K.S., Singh, U., et al. (2006). Circular chromosome conformation capture (4C) uncovers extensive networks of epigenetically regulated intra- and interchromosomal interactions. *Nat. Genet.* 38, 1341–1347.
- Zullo, J.M., Demarco, I.A., Piqué-Regi, R., Gaffney, D.J., Epstein, C.B., Spooner, C.J., Luperchio, T.R., Bernstein, B.E., Pritchard, J.K., Reddy, K.L., and Singh, H. (2012). DNA sequence-dependent compartmentalization and silencing of chromatin at the nuclear lamina. *Cell* 149, 1474–1487.